Available online at www.sciencedirect.com
ScienceDirect
Trans. Nonferrous Met. Soc. China 34(2024) 2192−2203
Transactions of Nonferrous Metals Society of China
www.tnmsc.cn

Microstructure and properties of K648 superalloy additively manufactured by extreme high-speed laser metal deposition

Kai-ming WANG[1,2], Wei LIU[1], Dong DU[2], Bao-hua CHANG[2], Guan LIU[3], Yong-le HU[1], Yong-gang TONG[1], Ming-jun ZHANG[1], Jian ZHANG[1], Jiang JU[4]

1. College of Automotive and Mechanical Engineering, Changsha University of Science and Technology, Changsha 410114, China;
2. State Key Laboratory of Tribology in Advanced Equipment, Department of Mechanical Engineering, Tsinghua University, Beijing 100084, China;
3. School of Mechanical and Electrical Engineering, Central South University, Changsha 410083, China;
4. Department of Materials Science and Engineering, City University of Hong Kong, Hong Kong 999077, China

Received 3 March 2023; accepted 9 November 2023

Abstract: In order to improve the manufacturing efficiency of high-chromium superalloys, an innovative extreme high-speed laser metal deposition (EHLMD) process was used. The growth behavior of precipitated phases, high-temperature mechanical properties, wear resistance, and corrosion resistance of EHLMD K648 superalloy were investigated and compared with conventional laser metal deposition (CLMD) using transmission electron microscope, tensile tester, wear tester and electrochemical workstation, respectively. The results reveal that the precipitated phase size in EHLMD K648 superalloy is significantly smaller than that in CLMD K648 superalloy. Moreover, EHLMD K648 superalloy demonstrates higher tensile strength at 700 °C, superior wear resistance, and excellent corrosion resistance compared to CLMD K648 superalloy. Consequently, the K648 superalloy manufactured through EHLMD technique exhibits favorable comprehensive properties.

Key words: additive manufacturing; extreme high-speed laser metal deposition (EHLMD); K648 superalloy; microstructure evolution; properties

1 Introduction

As industrial technology continues to advance, the demand for high-performance alloys has increased significantly, particularly for key high-temperature components in aero-engines, energy power, petrochemical, and nuclear power industries [1−3]. High chromium superalloy has been widely used in manufacturing hot-end parts in the above fields due to its good high-temperature oxidation resistance, corrosion resistance, and mechanical properties [4,5]. Overall metallurgical quality and manufacturing level are crucial factors influencing the longevity and reliability of equipment, making manufacturing technology a subject of extensive interest both domestically and internationally. High chromium superalloy has low yield, low thermo-plasticity, and poor hot workability due to its high chromium (Cr) content. The current processes encounter difficulties when manufacturing large and intricate parts, leading to subpar product quality that fails to meet requirements. These limitations severely impede the widespread adoption and utilization of high chromium superalloy parts [6]. Therefore, it is of

Corresponding author: Bao-hua CHANG, E-mail: bhchang@tsinghua.edu.cn; Jiang JU, E-mail: Jiang.Ju@cityu.edu.hk
DOI: 10.1016/S1003-6326(24)66534-9

great significance to develop a new manufacturing technology for large and complex high-chromium superalloy parts with high efficiency and excellent properties.

Additive manufacturing technology represents the latest advancement in manufacturing methodologies. It mainly includes selective laser melting (SLM), laser metal deposition (LMD), electron beam selective melting (EBSM), electron beam freeform fabrication (EBF) and wire and arc additive manufacturing (WAAM) [7−9]. SLM can be applied to preparing complex parts with high precision. However, its efficiency in producing larger parts is limited, and the manufacturing scope is restricted to small components. EBSM exhibits reduced thermal stress during the production of high-melting point materials, but it also suffers from low efficiency and limited forming size. EBF, while being capable of producing large-scale parts with high density, faces challenges related to precision, cost, and the necessity for a vacuum system. WAAM enables the processing of large-size components at a lower cost, yet it suffers from reduced part precision [10]. LMD can directly produce difficult-to-machine materials, significantly improving the yield of alloys and reducing production costs. Currently, the CLMD of typical superalloys (such as Inconel 718) has been explored, and the microstructure and properties of CLMD have been studied [11]. Nonetheless, further enhancements are required for the conventional LMD (CLMD) process due to its suboptimal utilization of laser energy and powder, as well as the relatively slow deposition rate. Extreme high-speed LMD (EHLMD) is a new high-efficiency additive manufacturing technology developed in recent years. Compared with CLMD, the deposition efficiency is significantly improved, which can also be improved from 50 to 500 cm^2/min [12]. This leads to a substantial reduction in the existence time of the melt pool, while linear scanning speeds can reach an impressive range of 10−200 m/min. Moreover, EHLMD boasts a higher proportion of laser energy acting on the powder in comparison to CLMD [13].

K648 represents a typical high chromium superalloy, known for its exceptional high-temperature mechanical properties, oxidation resistance, and corrosion resistance. As a result, it has found widespread use in the fabrication of hot-end components, such as aero-engine turbine blades [14,15]. The EHLMD, an innovative manufacturing technology, demonstrates the ability to efficiently produce challenging-to-machine materials directly. In order to explore the characteristics of EHLMD process, the EHLMD process of K648 superalloy is studied compared with CLMD process, and the microstructure and properties of K648 alloy deposited by EHLMD are revealed in this study. It is expected to provide a new technical method for the high quality and efficient manufacturing of high chromium superalloy parts and promote the development of EHLMD technology.

2 Experimental

The K648 superalloy powder utilized in this study was obtained through gas atomization from AMC Powders Co., Ltd. (China). The chemical composition of the powder is presented in Table 1. The particle size of the K648 superalloy powder for CLMD and EHLMD are 53−105 and 15−53 μm, respectively (see Fig. 1). Before the experiment, the K648 superalloy powder was dried for 4 h in a vacuum oven with a temperature of 120 °C. Additionally, the substrate surface was meticulously polished using sandpaper and subsequently cleaned with acetone to eliminate oil and oxide layers, ensuring proper surface preparation before conducting the CLMD and EHLMD experiments.

The CLMD experiment involved the use of specific equipment, comprising a fiber laser produced (YLS−6000), a pneumatic powder feeding system (BTSF−2) and an ABB six-axis robot system. CLMD process parameters are laser power of 2500 W, scanning speed of 0.24 m/min, powder feeding rate of 15 g/min, overlap rate of 50% and interlayer height of 0.7 mm. The equipment used in the EHLMD experiment mainly consists of an LDF−3000−40 laser produced by Laser line, an Oerlikon powder feeding system, and

Table 1 Chemical composition of K648 superalloy (wt.%)

Cr	Nb	Mo	Ti	Al	W	Fe	C	B	S	Ce	Ni
32.04	1.18	3.02	1.12	1.16	4.72	0.41	0.081	<0.001	<0.01	<0.03	Bal.

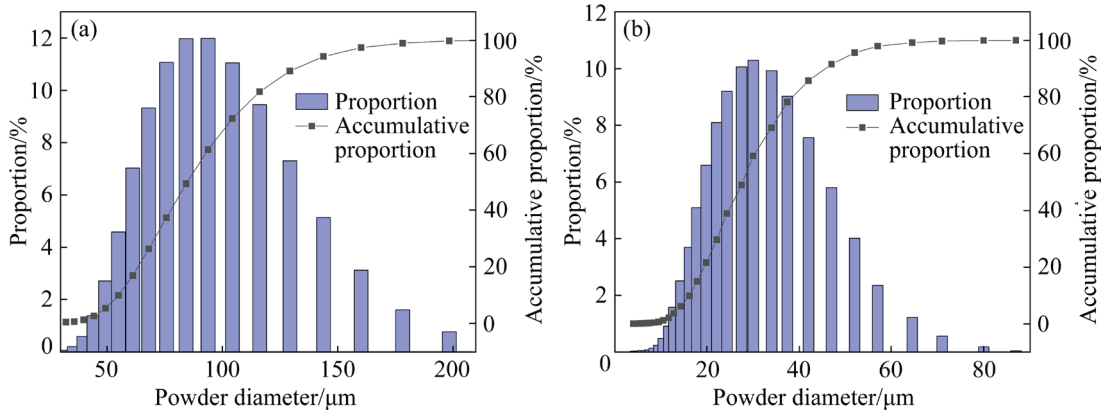

Fig. 1 Powder diameter distribution of K648 superalloy powder: (a) CLMD; (b) EHLMD

Table 2 CLMD and EHLMD process parameters

Process	Laser power/W	Scanning speed/ ($m \cdot min^{-1}$)	Powder feeding rate/($g \cdot min^{-1}$)	Overlap rate/%	Interlayer height/mm
CLMD	2500	0.24	15	50	0.7
EHLMD	1400	25	30	70	0.3

a CNC machine tool system. The process parameters for EHLMD are laser power of 1400 W, scanning speed of 25 m/min, powder feeding rate of 30 g/min, overlap rate of 70% and interlayer height of 0.3 mm. The CLMD and EHLMD process parameters are given in Table 2.

The phase composition of the K648 superalloy deposited through both CLMD and EHLMD was analyzed by Tecnai F30 TEM. An electronic universal testing machine (Instron 5582) was applied to the high-temperature tensile test at 700 °C, with a tensile rate of 0.1 mm/min. The size of the tensile sample is shown in Fig. 2. The tensile fracture morphology was analyzed by a field emission scanning electron microscope (GeminiSEM 300) to determine the fracture mechanism.

The wear test was carried out using Rtec MFT−5000 wear tester. The Si_3N_4 balls with a diameter of 6.35 mm were selected as the friction counterpart. The load used in the experiment was 20, 30, and 40 N. The frequency, reciprocating distance and the wear time were 1 Hz, 5 mm, 30 min, respectively. Meanwhile, the friction coefficients under different loads were recorded. After wear test, the wear volume and morphology of the samples under different loads were measured by laser confocal microscope. The worn surface morphology was observed by GeminiSEM300 field emission scanning electron microscope (SEM) to determine the wear mechanism of EHLMD K648 superalloy. The electrochemical corrosion

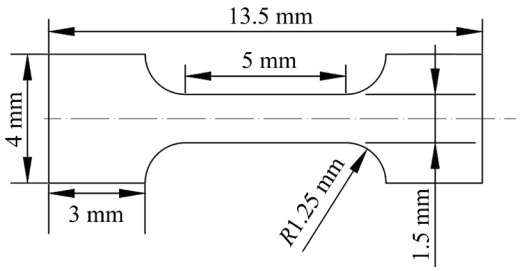

Fig. 2 Size of high-temperature tensile sample

performance of the CLMD and EHLMD K648 superalloy was tested via Gamry electrochemical workstation. The corrosion medium was 3.5 wt.% NaCl aqueous solution, and the test temperature was room temperature. The test was carried out using a three-electrode method, and the battery was composed of CLMD or EHLMD K648 superalloy, Ag/AgCl and Pt, representing working electrode, reference electrode, and counter electrode, respectively. Before the experiment, all the samples were immersed in NaCl aqueous solution for 1 h, and the function of open circuit potential (OCP) and time was measured. Until the OCP was stable, the polarization curve was measured at the scanning rate of 10 mV/s in the potential range from −0.4 to 2 V, and the test time was 1800 s. The corrosion potential and corrosion current density were obtained by extrapolation through the registration curve. Finally, the electrochemical impedance spectroscopy (EIS) was tested at the open circuit potential in the frequency range of 10^{-2}−10^5 Hz.

3 Results and discussion

3.1 Microstructure

The precipitated phase of EHLMD K648 superalloy analyzed by TEM is presented in Fig. 3. The EHLMD K648 superalloy has a large number of granular precipitates with a size of about 200 nm near the sub-grain boundaries. EDS results show that the phase is mainly composed of Cr elements (65.19 at.% Cr, 24.56 at.% Ni, 6.61 at.% Mo, and 3.62 at.% W). According to the standard phase in ICSD database, this phase is identified as the α-Cr phase, characterized by a BCC structure. Furthermore, it is observed that the size of the α-Cr phase in the EHLMD K648 superalloy is significantly smaller than that in the CLMD K648 superalloy (see Fig. 3(c)). The diffraction spots of the matrix shows that the matrix is mainly γ-Ni. No γ' phase is found in the matrix of γ-Ni. This absence of γ' phase might be attributed to the low content of elements required for γ' phase formation in the K648 powder, resulting in an insufficient concentration of these elements. A similar phenomenon was observed by CHENG et al [16] who prepared GH648 superalloy via selective laser melting (SLM). In both cases, the absence of γ' phase is associated with the solidification characteristics of the melt pool, which are comparable between EHLMD process and SLM, characterized by high scanning speeds and rapid cooling rates. It is found that the precipitated phase of EHLMD K648 superalloy is mainly the α-Cr phase, and the size of the precipitated phase is obviously smaller than that of CLMD K648 superalloy, which is related to the high scanning speed and rapid cooling rate in the EHLMD process. Additionally, a limited number of dislocations are identified within the matrix of the EHLMD K648 superalloy, though their prevalence is lower compared to that in the CLMD K648 superalloy.

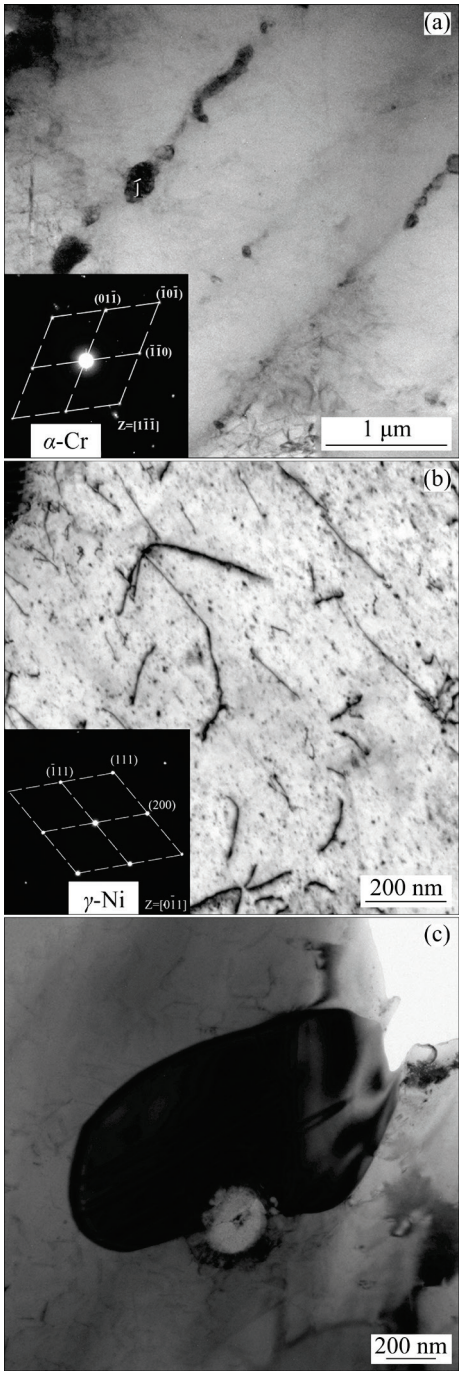

Fig. 3 TEM images of K648 superalloy deposited by EHLMD and CLMD: (a) α-Cr in EHLMD K648 superalloy; (b) γ-Ni in EHLMD K648 superalloy; (c) α-Cr in CLMD K648 superalloy

3.2 High-temperature tensile property

The previous research showed that EHLMD K648 superalloy has better room-temperature ultimate strength (883.4 MPa) than CLMD K648 superalloy (833 MPa) [17]. Based upon this, the high-temperature mechanical properties of CLMD and EHLMD K648 superalloy are investigated in this study. Figure 4 illustrates the tensile curves of CLMD and EHLMD K648 superalloy at 700 °C. The ultimate tensile strength of CLMD K648 superalloy is about 434.8 MPa, and the elongation is about 58.1%. However, the ultimate tensile strength of EHLMD K648 superalloy is about 773.5 MPa, and the elongation is about 16.5%. These results clearly indicate that the EHLMD K648 superalloy demonstrates a superior ability to retain its strength at high temperatures compared to

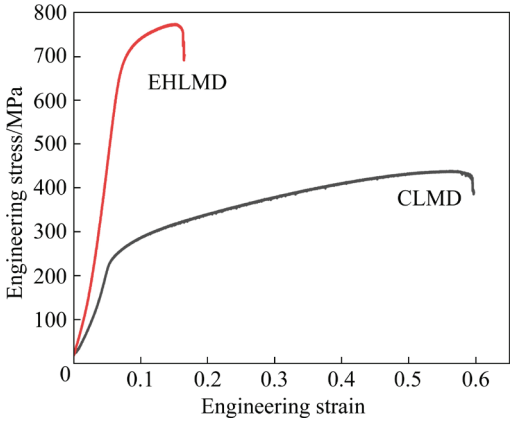

Fig. 4 Tensile curves of CLMD and EHLMD K648 superalloy at 700 °C

the CLMD K648 superalloy. The observed differences in the mechanical properties of the CLMD and EHLMD K648 superalloys can be attributed to their respective microstructures. Due to the high-temperature gradient and faster cooling rate in the EHLMD process, the grain of EHLMD K648 superalloy is significantly smaller than that of CLMD K648 superalloy. On the other hand, the size of the α-Cr phase in EHLMD is smaller, the distribution in the matrix is more uniform, and the second phase strengthening effect is more obvious than that of CLMD K648 superalloy. In summary, the EHLMD K648 superalloy exhibits superior high-temperature strength due to its distinct microstructural characteristics, which is reflected in the smaller grain size and more effective second-phase strengthening effect compared to the CLMD K648 superalloy.

To further investigate the fracture mechanism of EHLMD K648 superalloy at high temperature, the fracture morphologies of EHLMD and CLMD K648 superalloy observed by SEM are illustrated in Fig. 5. The fracture surface is mainly dominated by dimples, which indicates that the fracture mode of CLMD and EHLMD K648 superalloy at high temperature is mainly ductile fracture. The fracture morphology of CLMD K648 superalloy (Fig. 5(a)) is mainly composed of thick and flat dimples, which indicates that CLMD K648 superalloy experiences greater deformation in the tensile process, and it has better plasticity. On the other hand, the fracture morphology of EHLMD K648 superalloy (Fig. 5(b)) primarily comprises small dimples, indicating that its plasticity is lower than that of the CLMD K648 superalloy.

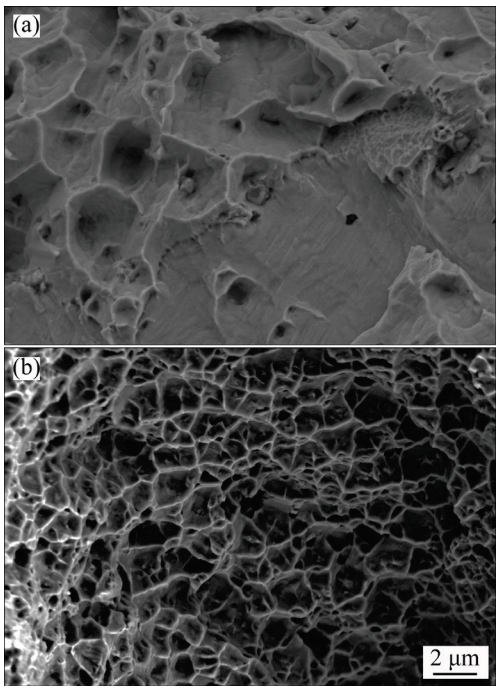

Fig. 5 Fracture morphologies of K648 superalloy at 700 °C: (a) CLMD; (b) EHLMD

3.3 Wear resistance

The wear volumes of both CLMD and EHLMD K648 superalloys measured under various loads using a laser confocal microscope are presented in Fig. 6(a). It is evident that the wear volume of CLMD and EHLMD K648 superalloy increases with the increasing wear loads. The wear volume of EHLMD K648 superalloy is lower than that of CLMD K648 superalloy under the same wear load, indicating that the wear resistance of EHLMD K648 superalloy is superior to that of CLMD K648 superalloy. The wear rates (ω, $mm^3 \cdot N^{-1} \cdot s^{-1}$) of the CLMD and EHLMD K648 superalloy under different loads can be calculated by the change of wear volume [18]:

$$\omega = \frac{V}{P \cdot t} \tag{1}$$

where V (mm^3) is the wear volume, P (N) represents the wear load, and t (s) denotes the wear time.

The wear rates of CLMD and EHLMD K648 superalloy under different loads are calculated (see Fig. 6(b)). The wear rate of EHLMD K648 superalloy is lower than that of the CLMD K648 superalloy under different loads, and the wear rates of the CLMD and EHLMD K648 superalloy increase with the increase of load. This finding is

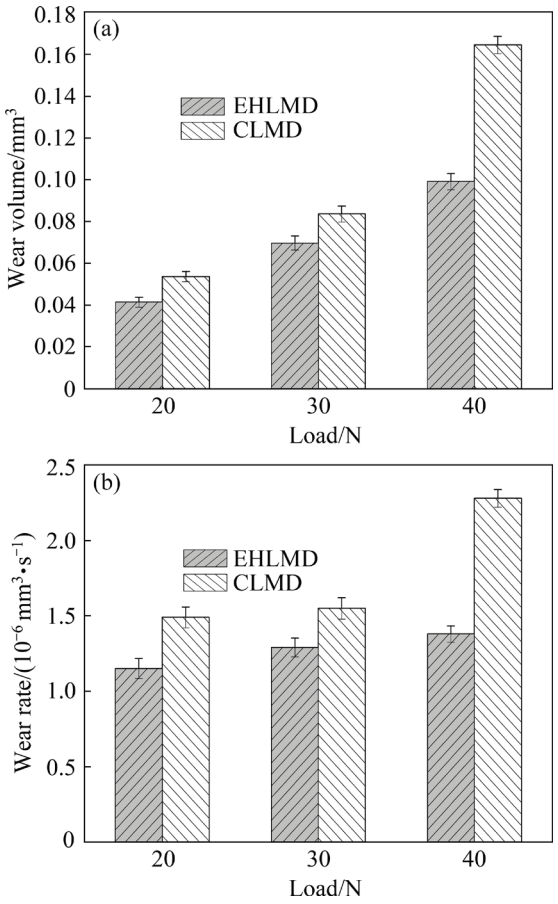

Fig. 6 Wear volumes (a) and wear rates (b) of CLMD and EHLMD K648 superalloy under different loads

essential in determining the suitability of EHLMD K648 superalloy for wear-resistant applications, highlighting its potential advantages over the CLMD K648 superalloy in such scenarios.

The enhanced wear resistance of the EHLMD K648 superalloy can be attributed to the significant reduction in grain size compared to the CLMD K648 superalloy. The smaller the grain size, the better the effect of fine-grain strengthening. According to our previous study, the average microhardness of EHLMD K648 superalloy and CLMD K648 superalloy are HV 298.1 and HV 220.5, respectively. That is to say, the higher the hardness, the stronger the wear resistance of the alloy. On the other hand, the higher cooling rate during the EHLMD process leads to a smaller size and more uniform distribution of the α-Cr precipitated phase in the alloy. This refinement of the microstructure contributes to the hardening of the alloy, resulting in enhanced wear resistance.

Figure 7 shows the coefficients of friction (COF) of CLMD and EHLMD K648 superalloy under different loads. The COF of EHLMD K648 superalloy basically changes in a relatively small range under different loads, and the COF increases at first and then decreases with increasing load. The COF of CLMD K648 superalloy increases slightly with increasing load. The COF of CLMD K648 superalloy is higher than that of EHLMD K648 superalloy under different loads. It is further confirmed that the wear resistance of K648 superalloy deposited by EHLMD is slightly higher than that of CLMD K648 superalloy.

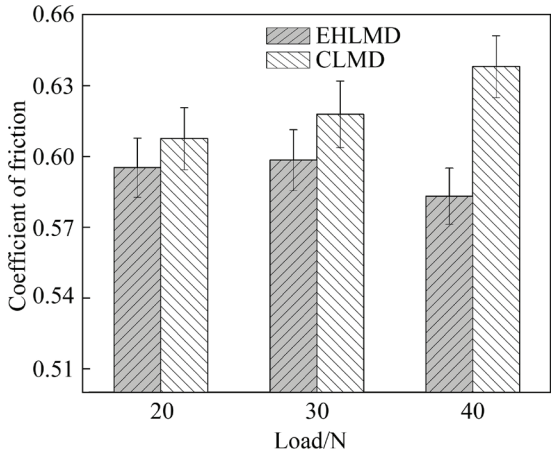

Fig. 7 Coefficients of friction of CLMD and EHLMD K648 superalloy under different loads

Figure 8 displays the 3D morphology of wear tracks for both CLMD and EHLMD K648 superalloy under different loads measured by laser confocal microscopy. Figure 9 presents the profile of the cross-sectional width and depth of the wear tracks under different loads. It can be seen from Figs. 8 and 9 that under the load of 20 N, the maximum depth and width of wear tracks of EHLMD K648 superalloy are 0.026 and 0.894 mm, respectively, which are slightly lower than those of 0.029 and 0.951 mm of CLMD K648 superalloy. With the increase of load to 30 N, the maximum depth and width of wear tracks of EHLMD K648 superalloy increase to 0.040 and 1.032 mm, increased by 53.8% and 15.4%, respectively, while the maximum depth and width of CLMD K648 superalloy increase to 0.045 and 1.119 mm, by 55.2% and 17.6%, respectively. Upon further increasing the load to 40 N, the maximum depth and width of wear tracks of EHLMD K648 superalloy further increase to 0.054 and 1.173 mm, by 20% and 13.7%, respectively, while the maximum depth and width of CLMD K648 superalloy

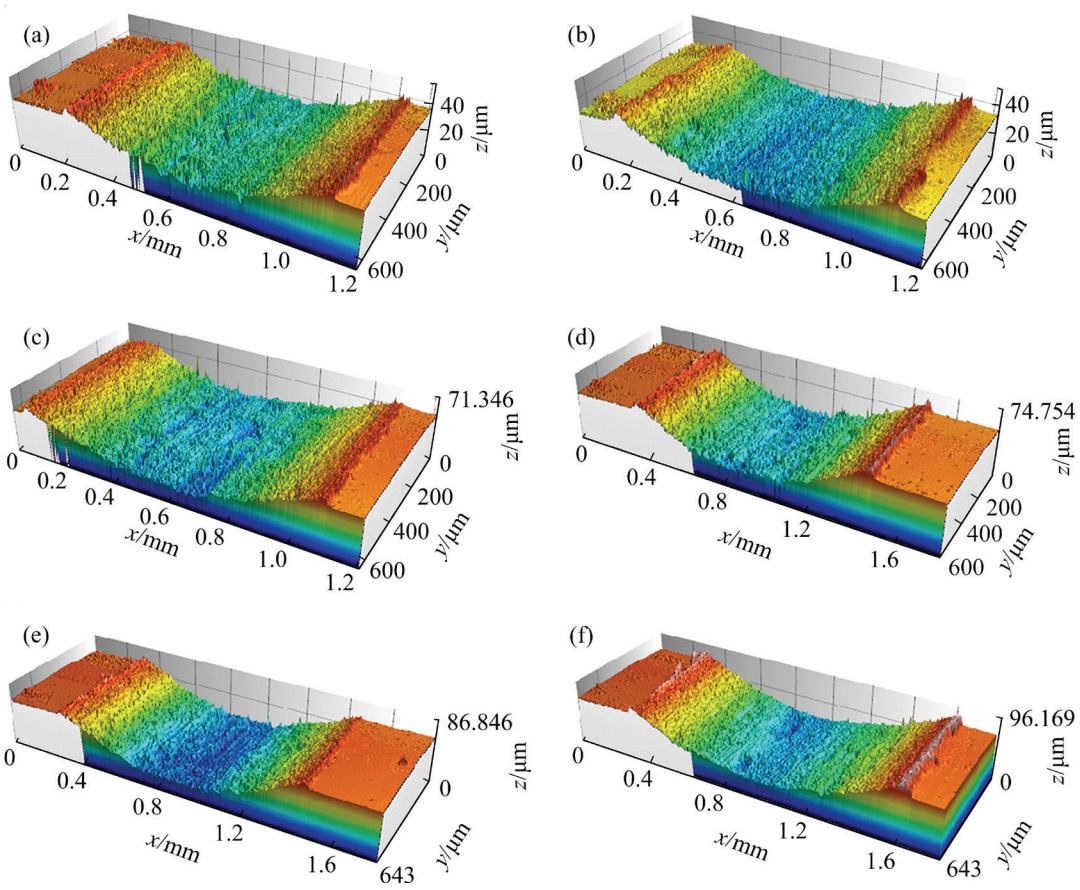

Fig. 8 3D morphologies of wear tracks of EHLMD (a, c, e) and CLMD (b, d, f) K648 superalloy under different loads: (a, b) 20 N; (c, d) 30N; (e, f) 40N

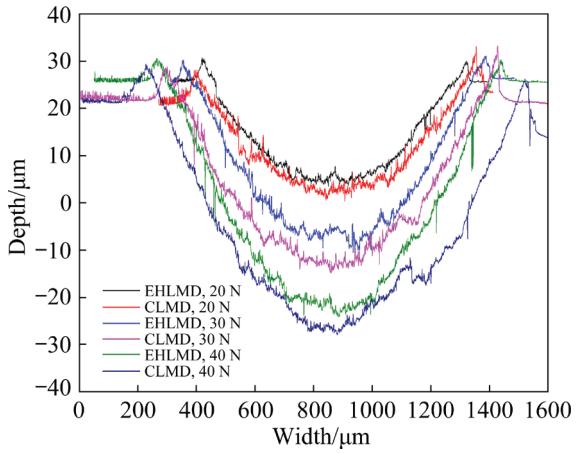

Fig. 9 Profiles of cross-sectional width and depth of wear tracks of CLMD and EHLMD K648 superalloy under different loads

wear tracks further increase to 0.058 and 1.519 mm, by 28.9% and 35.7%, respectively. Above results show that the maximum depth and width of wear tracks of CLMD K648 superalloy are larger than those of EHLMD K648 superalloy under different loads. Moreover, the increase ratio of the maximum depth and width of wear tracks of EHLMD K648 superalloy is lower than that of CLMD K648 superalloy with the increase in load. These findings further indicate that the wear resistance of EHLMD K648 superalloy is superior to that of CLMD K648 superalloy.

Figure 10 presents the worn surface morphologies of CLMD and EHLMD K648 superalloy under different loads. The worn surfaces of both CLMD and EHLMD K648 superalloys are mainly composed of furrow and debris, indicating that the dominant wear mechanisms of both CLMD and EHLMD K648 superalloys are mainly abrasive wear and adhesive wear. There are white debris on the worn surface of EHLMD K648 superalloy, and its amount increases gradually with the increase of load. EDS analysis of the white debris (Area 1) reveals that it predominantly comprises 59.47 at.% O, 21.83 at.% Ni, 12.78 at.% Cr, 2.49 at.% Si, 1.16 at.% Al, 0.74 at.% Mo, and 0.59 at.% Ti. This composition indicates that the white debris is primarily oxide-based. This is mainly due to the

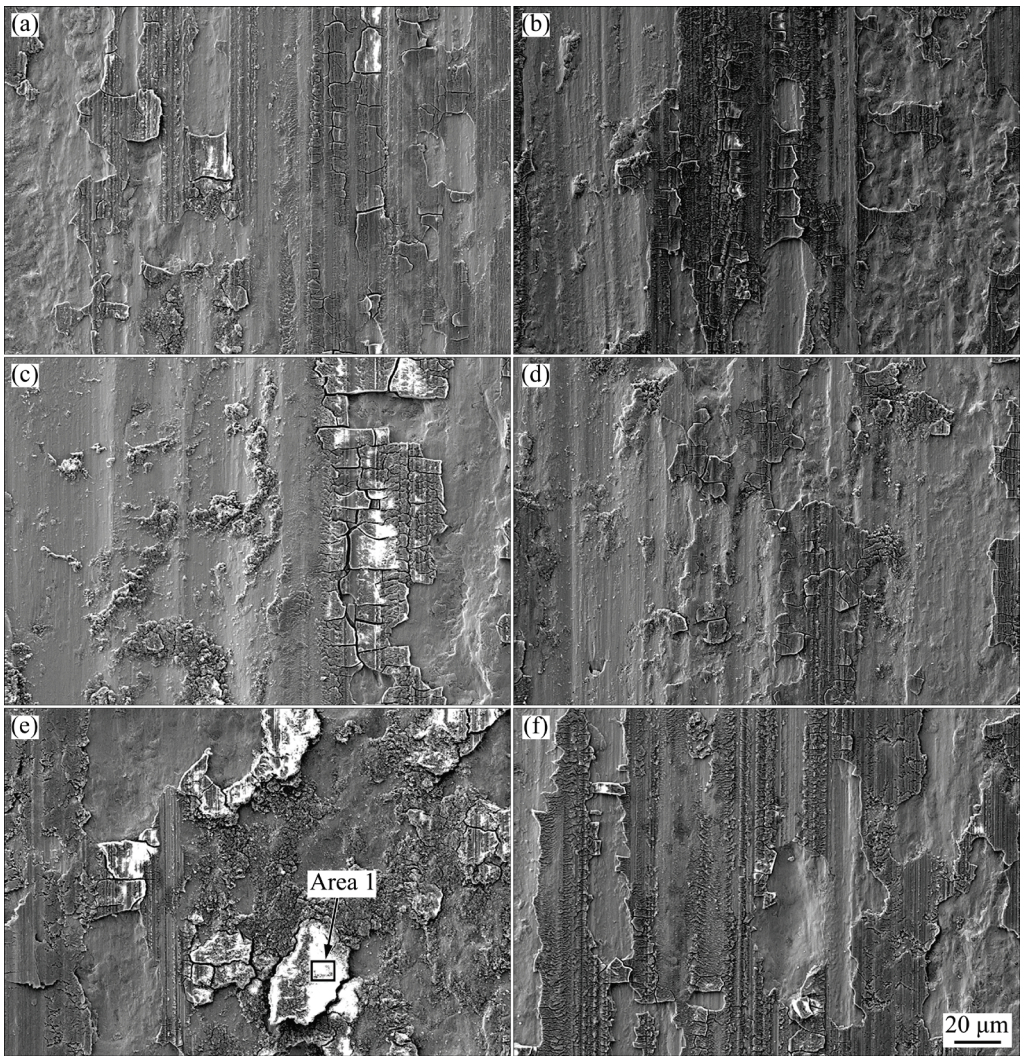

Fig. 10 Worn surface morphologies of EHLMD (a, c, e) and CLMD (b, d, f) K648 superalloy under different loads: (a, b) 20 N; (c, d) 30 N; (e, f) 40 N

heat generated by friction between the matrix and the grinding ball during the wear process, which leads to a certain oxidation on the wear surface. As the load increases, the pressure on the matrix intensifies, leading to a corresponding increase in the amount of oxide debris on the worn surface. Furthermore, the number and size of furrows corresponding to EHLMD K648 superalloy under various loads are less than those of CLMD K648 superalloy. This difference can be attributed to the microstructure of two K648 superalloys. The EHLMD K648 superalloy possesses a smaller grain size and more fine precipitates, contributing to its relatively higher microhardness. During the wear process, the precipitated phase strengthens the matrix and has a stronger ability to resist the pressure of abrasive particles on the surface of the alloy. Consequently, EHLMD K648 superalloy exhibits higher wear resistance, with fewer and smaller furrows compared to the CLMD K648 superalloy.

3.4 Corrosion resistance

The polarization curves of EHLMD and CLMD K648 superalloy are shown in Fig. 11. The self-corrosion potential of EHLMD K648 superalloy is −0.430 V and that of CLMD K648 superalloy is −0.423 V. Generally, higher corrosion current density of an alloy indicates a faster corrosion rate of the material [19]. The corrosion current densities of EHLMD K648 superalloy and CLMD K648 superalloy were fitted by linear extrapolation method, and the results are summarized in Table 3. The corrosion current density

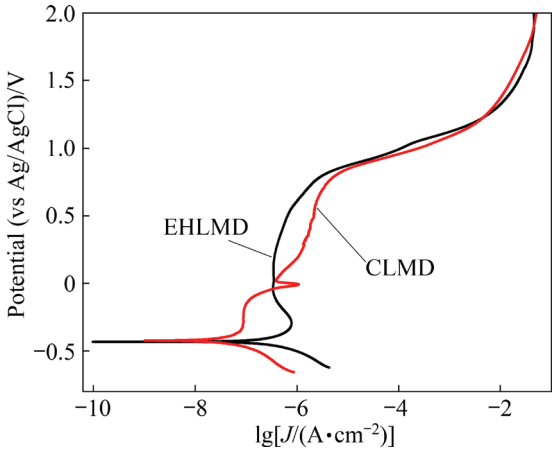

Fig. 11 Polarization curves of EHLMD and CLMD K648 superalloy

Table 3 Corrosion parameters of EHLMD and CLMD K648 superalloy

Sample	Corrosion potential (vs Ag/AgCl)/V	Corrosion current density/(A·cm^{-2})
EHLMD	−0.430	5.692×10^{-7}
CLMD	−0.423	1.218×10^{-7}

of EHLMD K648 superalloy is higher than that of CLMD K648 superalloy, indicating that the corrosion rate of EHLMD K648 superalloy is comparatively higher than that of CLMD K648 superalloy. However, it is noteworthy that the corrosion current density of both CLMD and EHLMD K648 superalloys is significantly lower than that of SLM Inconel 718 superalloy (3.18×10^{-6} A/cm^2) [20]. This observation highlights that the K648 superalloys prepared through these two processes exhibit excellent corrosion resistance.

Electrochemical impedance spectroscopy (EIS) testing is commonly employed to study the corrosion evolution of metal alloy materials [21]. In this study, the effects of CLMD and EHLMD on the corrosion resistance of K648 superalloy were investigated. As depicted in the Nyquist diagram (see Fig. 12(a)), the capacitive arc radius of CLMD K468 superalloy is larger than that of EHLMD K468 superalloy. A larger capacitive arc radius signifies higher charge transfer resistance, indicating a lower corrosion rate during the corrosion process and, consequently, better corrosion resistance [22,23]. Experimental results show that the corrosion resistance of CLMD K648 superalloy is better than that of EHLMD K468 superalloy. The $R_s(R_{ct}Q)$ model is used to fit the impedance spectrum of the test samples, as inserted in Fig. 12(a). Fitting results are given in Table 4, where $\sum\chi^2$ is the fitting error, the constant phase angle element (CPE) is used to replace the capacitive element, and n is the exponential term in the constant phase angle element. It can be seen from Table 4 that the charge transfer resistance R_{ct} of CLMD K468 alloy is 2.84 times that of EHLMD

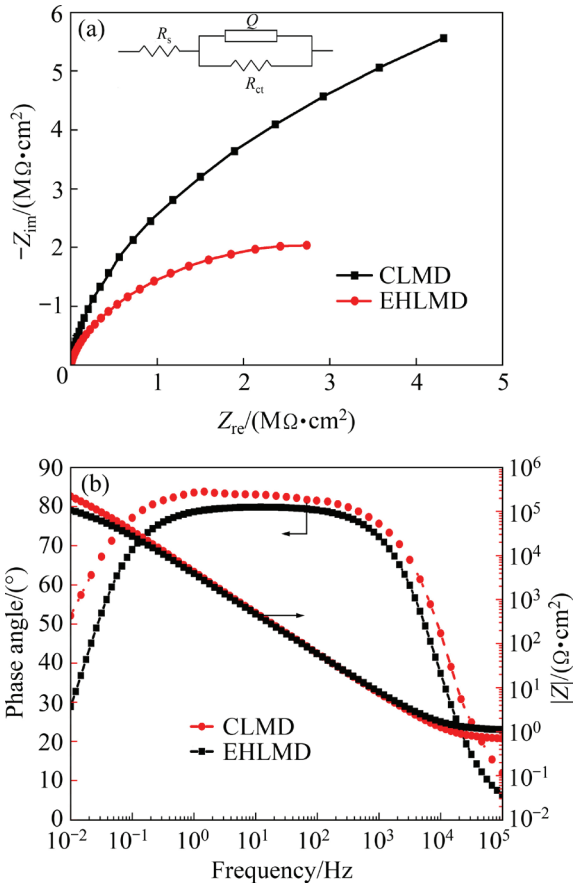

Fig. 12 Electrochemical impedance spectra of CLMD and EHLMD K648 superalloy: (a) Nyquist diagram; (b) Bode diagram

Table 4 Equivalent circuit parameters of CLMD and EHLMD K648 superalloy

Sample	R_s/(Ω·cm^2)	CPE/(Ω^{-1}·s^n·cm^{-2})	n	R_{ct}/(Ω·cm^2)	$\sum\chi^2$
EHLMD	1.127	5.287×10^{-5}	0.8906	1.38×10^5	2.2×10^{-3}
CLMD	0.7043	4.32×10^{-5}	0.9192	3.92×10^5	1.3×10^{-3}

K468 alloy. This observation indicates that the charge transfer resistance of the CLMD K648 superalloy is higher, suggesting a stronger passivation film resistance and, consequently, better corrosion resistance.

The EHLMD K648 superalloy exhibits favorable corrosion resistance; however, the corrosion resistance of the presently prepared EHLMD K648 superalloy appears marginally inferior to that of the CLMD K648 superalloy. This disparity can be attributed to the fact that the grain size of the EHLMD K648 superalloy is finer compared to CLMD K648 superalloy, resulting in a larger boundary area. The higher energy at the grain boundary renders the atoms in an unstable state, making the alloy susceptible to corrosion at these boundaries [24]. Consequently, the increase in grain boundary area caused by grain refinement contributes to a reduction in the corrosion resistance of the EHLMD K648 superalloy. Moreover, based on our previous research, the porosity of EHLMD K648 superalloy is higher than that of CLMD K648 superalloy [25], and the higher porosity makes it easier for corrosive media to invade the matrix [26]. Therefore, the corrosion resistance of EHLMD K648 superalloy is slightly lower than that of CLMD K648 superalloy.

4 Conclusions

(1) The precipitated phase size of EHLMD K648 superalloy is significantly smaller than that of CLMD K648 superalloy.

(2) EHLMD K648 superalloy demonstrates superior strength retention capability compared to CLMD at high temperature of 700 °C.

(3) The wear resistance of EHLMD K648 superalloy surpasses that of CLMD K648 superalloy.

(4) The EHLMD K648 superalloy has good corrosion resistance, but the self-corrosion current density is slightly higher than that of CLMD K648 superalloy.

CRediT authorship contribution statement

Kai-ming WANG: Conceptualization, Formal analysis, Writing − Original draft, Writing − Original draft preparation, Methodology, Data curation, Funding acquisition; **Wei LIU:** Conceptualization, Formal analysis, Writing − Original draft, Writing − Original draft preparation; **Dong DU:** Data analysis, Writing − Review and editing; **Bao-hua CHANG:** Conceptualization, Formal analysis, Writing − Original draft, Methodology, Data curation, Funding acquisition, Project administration and supervision; **Guan LIU:** Data analysis, Writing − Review and editing; **Yong-le HU:** Data analysis, Writing − Review and editing; **Yong-gang TONG:** Data analysis, Writing − Review and editing; **Ming-jun ZHANG:** Data analysis, Writing − Review and editing; **Jian ZHANG:** Data analysis, Writing − Review and editing; **Jiang JU:** Writing − Original draft preparation, Project administration and supervision.

Declaration of competing interest

The authors declare that they have no known competing financial interests or personal relationships that could have appeared to influence the work reported in this paper.

Acknowledgments

The authors would like to acknowledge the financial support for this work from the National Natural Science Foundation of China (No. 52205334), the Natural Science Foundation of Hunan Province, China (No. 2022JJ40495), the Changsha Key Research and Development Project, China (No. kh2201275), the Changsha Municipal Natural Science Foundation, China (No. kq2202196), and the Tribology Science Fund of State Key Laboratory of Tribology in Advanced Equipment, China (No. SKLTKF21B08).

References

[1] GU Dong-dong, SHI Xin-yu, POPRAWE R, BOURELL D, SETCHI R, ZHU Ji-hong. Material−structure−performance integrated laser-metal additive manufacturing [J]. Science, 2021, 372(6545): 1487.

[2] XUE Jun-liang, GUO Wei, YANG Jin, XIA Ming-sheng, ZHAO Guang, TAN Cai-wang, WAN Zhan-dong, CHI Jia-xuan, ZHANG Hong-qiang. In-situ observation of microcrack initiation and damage nucleation modes on the HAZ of laser-welded DP1180 joint [J]. Journal of Materials Science & Technology, 2023, 148: 138−149.

[3] LI Yang, KAN Wen-bin, ZHANG Yan-ming, LI Ming-zhi, LIANG Xiao-yu, YU Ye-feng, LIN Feng. Microstructure, mechanical properties and strengthening mechanisms of IN738LC alloy produced by Electron Beam Selective Melting [J]. Additive Manufacturing, 2021, 47: 102371.

[4] WANG Kai-ming, LIU Wei, DU Dong, CHANG Bao-hua, PANG Xiao-tong, HU Yong-le, TONG Yong-gang, FU Han-guang, JU Jiang. Microstructure evolution and mechanical properties of high-chromium superalloy

manufacturing by extreme high-speed laser metal deposition at different aging temperatures [J]. Journal of Alloys and Compounds, 2023, 969: 172202.

[5] RAPETTI A, CHRISTIEN F, TANCRET F, TODESCHINI P, HENDILI S, STODOLNA J. Surfactant effect of impurity sulphur in ductility dip cracking of a high-chromium nickel model alloy [J]. Scripta Materialia, 2021, 194: 113680.

[6] KESKAR N, PATTANAIK A K, MANI KRISHNA K V, SRIVASTAVA D, DEY G K. Kinetics and grain boundary selectivity of discontinuous precipitation in binary Ni−Cr alloy [J]. Metallurgical and Materials Transactions A, 2017, 48(6): 3096−3107.

[7] LI Yan-peng, WANG Chang-rui, DU Xiao-dong, TIAN Wei, ZHANG Tao, HU Jun-shan, LI Bo, LI Peng-cheng, LIAO Wen-he. Research status and quality improvement of wire arc additive manufacturing of metals [J]. Transactions of Nonferrous Metals Society of China, 2023, 33(4): 969−996.

[8] LAI Yi, DENG Ying, ZHU Xin-wen, GUO Yi-fan, XU Guo-fu, HUANG Ji-wu, YIN Zhi-min. Tensile property and microstructure of Al−4.77Mn−1.37Mg−0.67Sc−0.25Zr alloy under different selective laser melting processing parameters [J]. Transactions of Nonferrous Metals Society of China, 2023, 33(2): 357−370.

[9] WEN Yan, SUN Xuan, ZHOU Jian, LIU Bing-liang, GUO Hao-jie, LI Yu-xin, YIN Fei, WANG Li-qiang, XIE Le-chun, HUA Lin. Influence of electroshocking treatment on microstructure and mechanical properties of Ti−6.5Al−3.5Mo−1.5Zr−0.3Si thin-wall specimen manufactured by laser melting deposition [J]. Acta Metallurgica Sinica (English Letters), 2024, 37: 145−158.

[10] DEBROY T, WEI H L, ZUBACK J S, MUKHERJEE T, ELMER J W, MILEWSKI J O, BEESE A M, WILSON H A, DE A, ZHANG W. Additive manufacturing of metallic components – Process, structure and properties [J]. Progress in Materials Science, 2018, 92: 112−224.

[11] YUAN Kang-bo, GUO Wei-guo, LI Pen-ghui, WANG Jian-jun, SU Yu, LIN Xin, LI Yan-ping. Influence of process parameters and heat treatments on the microstructures and dynamic mechanical behaviors of Inconel 718 superalloy manufactured by laser metal deposition [J]. Materials Science and Engineering A, 2018, 721: 215−225.

[12] SCHOPPHOVEN T, GASSER A, BACKES G. EHLA: Extreme high‐speed laser material deposition: Economical and effective protection against corrosion and wear [J]. Laser Technik Journal, 2017, 14(4): 26−29.

[13] YUAN Wu-yan, LI Rui-feng, CHEN Zhao-hui, GU Jia-yang, TIAN Ying-tao. A comparative study on microstructure and properties of traditional laser cladding and high-speed laser cladding of Ni45 alloy coatings [J]. Surface and Coatings Technology, 2021, 405: 126582.

[14] BI Zhong-nan, DONG Jian-xin, ZHENG Lei, XIE Xi-shan. Phenomenon and mechanism of high temperature low plasticity in high-Cr nickel-based superalloy [J]. Journal of Materials Science & Technology, 2013, 29: 187−192.

[15] ZHENG Liang, XIAO Cheng-bo, ZHANG Guo-qing, GU Guo-hong, TANG Ding-zhong. Key factors in quality control of a high Cr content cast Ni-base superalloy K4648 [J]. Rare Metals, 2011, 30(Supp1.): 410−413.

[16] CHENG Bo-wen, GU Ji, SONG Min. An investigation of the microstructural evolution and tensile properties of a nickel-based GH648 superalloy manufactured through selective laser melting [J]. Materials Science and Engineering A, 2020, 790: 139704.

[17] WANG Kai-ming, DU Dong, LIU Guan, PU Ze, CHANG Bao-hua, JU Jiang. A study on the additive manufacturing of a high chromium Nickel-based superalloy by extreme high-speed laser metal deposition [J]. Optics & Laser Technology, 2021, 133: 106504.

[18] MUNAGALA V N V, BESSETTE S, GAUVIN R, CHROMIK R R. Sliding wear of cold sprayed Ti6Al4V coatings: Effect of porosity and normal load [J]. Wear, 2020, 450/451: 203268.

[19] LUO Guo-yun, XIAO Hui, LI Si-meng, WANG Cun-shan, ZHU Qiang, SONG Li-jun. Quasi-continuous-wave laser surface melting of aluminium alloy: Precipitate morphology, solute segregation and corrosion resistance [J]. Corrosion Science, 2019, 152: 109−119.

[20] LUO Shun-cun, HUANG Wen-pu, YANG Hui-hui, YANG Jing-jing, WANG Ze-min, ZENG Xiao-yan. Microstructural evolution and corrosion behaviors of Inconel 718 alloy produced by selective laser melting following different heat treatments [J]. Additive Manufacturing, 2019, 30: 100875.

[21] YAN Xiao-lei, GUO Hui, YANG Wei, PANG Shu-jie, WANG Qing, LIU Ying, LIAW P K, ZHANG Tao. $Al_{0.3}Cr_xFeCoNi$ high-entropy alloys with high corrosion resistance and good mechanical properties [J]. Journal of Alloys and Compounds, 2021, 860: 158436.

[22] CHEN Lin, BAI Shu-lin, GE Yang-yang, WANG Qin-ying. Erosion-corrosion behavior and electrochemical performance of Hastelloy C22 coatings under impingement [J]. Applied Surface Science, 2018, 456: 985−998.

[23] LIU Qu, MA Qing-xian, CHEN Gao-qiang, CAO Xiong, ZHANG Shuai, PAN Ji-luan, ZHANG Gong, SHI Qing-yu. Enhanced corrosion resistance of AZ91 magnesium alloy through refinement and homogenization of surface microstructure by friction stir processing [J]. Corrosion Science, 2018, 138: 284−296.

[24] RALSTON K D, BIRBILIS N, DAVIES C H J. Revealing the relationship between grain size and corrosion rate of metals [J]. Scripta Materialia, 2010, 63: 1201−1204.

[25] WANG Kai-ming, DU Dong, LIU Guan, PU Ze, CHANG Bao-hua, JU Jiang. High-temperature oxidation behaviour of high chromium superalloys additively manufactured by conventional or extreme high-speed laser metal deposition [J]. Corrosion Science, 2020, 176: 108922.

[26] WU J, ZHANG S D, SUN W D, GAO Y, WANG J Q. Enhanced corrosion resistance in Fe-based amorphous coatings through eliminating Cr-depleted zones [J]. Corrosion Science, 2018, 136: 161−173.

超高速激光金属沉积增材制造 K648 高温合金的显微组织与性能

王开明[1,2]，刘 炜[1]，都 东[2]，常保华[2]，刘 冠[3]，
胡永乐[1]，仝永刚[1]，张明军[1]，张 健[1]，鞠 江[4]

1. 长沙理工大学 汽车与机械工程学院，长沙 410114；
2. 清华大学 机械工程系 高端装备界面科学与技术全国重点实验室，北京 100084；
3. 中南大学 机电工程学院，长沙 410083；
4. 香港城市大学 材料科学与工程系，香港 999077

摘 要：采用一种新型的超高速激光金属沉积工艺以提高高铬高温合金的制造效率。分别使用透射电子显微镜、拉伸试验机、磨损试验机和电化学工作站对超高速激光金属沉积高铬 K648 高温合金的析出相生长行为、高温力学性能、耐磨性和耐腐蚀性进行研究，并与传统激光金属沉积工艺进行比较。结果表明，超高速激光金属沉积 K648 合金的析出相尺寸明显小于传统激光金属沉积工艺制备的 K648 合金，700 ℃下的高温强度更高，且具有良好的耐磨性和耐腐蚀性。总之，超高速激光金属沉积制造的 K648 高铬高温合金具有良好的综合性能。

关键词：增材制造；超高速激光金属沉积；K648 高温合金；显微组织演变；性能

(Edited by Bing YANG)